Thesis for the degree of Licentiate of Engineering

Structure and Dynamics in Ionic Liquid and Highly Concentrated Electrolytes

FILIPPA LUNDIN

Department of Physics
Chalmers University of Technology
Göteborg, Sweden 2020

Structure and Dynamics in Ionic Liquid and Highly Concentrated Electrolytes
FILIPPA LUNDIN

Department of Physics
Chalmers University of Technology
SE-412 96 Gothenburg
Sweden
Telephone +46 (0)31-772 1000

Chalmers, Chalmers digitaltryck
Gothenburg, Sweden 2020

Structure and Dynamics in Ionic Liquid and Highly Concentrated Electrolytes

Filippa Lundin, Department of Physics, Chalmers University of Technology, SE-41296 Göteborg, Sweden

Abstract

The electrolyte is a crucial part of a battery in terms of longevity and safety. However, the state-of-the-art electrolytes for lithium-ion batteries are based on organic solvents and Li-salts (typically 1M concentration) and are known to be volatile and to degrade at higher temperature. In the search for a safer electrolyte, highly concentrated electrolytes (HCEs) and ionic liquids (ILs) have been proposed as alternatives. The high salt concentration in HCEs (typically >4M) results in an increased electrochemical stability whereas ionic liquids, consisting only of ions, are known to have a negligible vapour pressure and high thermal stability. A common feature for HCEs and ILs is an ordering on mesoscopic length scales, normally not found in simple liquids, resulting from correlations between the ions. This nanostructure can be expected to influence the ion transport and a key to develop these new electrolyte concepts is to understand the structure and dynamics on the molecular level and how this links to macroscopic transport properties.

The thesis focuses on the understanding of mesoscopic structure and dynamics in ILs and HCEs with the help of neutron and X-ray scattering with the aim to identify how local dynamical processes are influenced by the nanostrucutre. I have investigated an archetypal HCE system where the Li-salt LiTFSI is dissolved in acetonitrile and a model ionic liquid. Varying the Li-salt concentration in the HCE we can link the local processes to the development of the structure. The ion transport in the HCE takes place by the means of a jump diffusion and is highly dependent on the salt concentration and temperature of the system. For the ionic liquid we investigate the response of structure and dynamics to changes in both pressure and temperature with a particular focus on state points (P,T) where the macroscopic dynamics i.e. conductivity is constant. A confined diffusion was found with a diffusion coefficient in agreement with macroscopic conductivity, thus providing a link between the microscopic and macroscopic dynamics.

Keywords: Ionic Liquid, Electrolytes, Highly concentrated electrolytes, QENS, SAXS.

List of Papers

This thesis is based on the following papers:

I *Density scaling of structure and dynamics of an ionic liquid*
H.W. Hansen, F. Lundin, K. Adrjanowicz, B. Frick, A. Matic, K. Niss
Physical Chemistry Chemical Physics **2020**, *22*, 1463-9076.

II *Local dynamics and nanostructure of an ionic liquid under pressure as a function of temperature*
F. Lundin, H.W. Hansen, B. Frick, D. Rauber, R. Hempelmann, O. Shebanova, K. Niss, A. Matic
Manuscript

III *Structure and dynamics in highly concentrated electrolytes*
F. Lundin, L. Aguilera, H.W. Hansen, B. Frick, S. Lages, A. Labrador, K. Niss, A. Matic
Manuscript

Contribution Report

I I planned the SAXS experiment that was performed together with co-authors and took part in the QENS experiment. I contributed to the discussion of results and writing of the paper.

II I planned the SAXS experiment that was performed together with co-authors and took part in the QENS experiment. I performed all data analysis and wrote the first draft of the paper.

III I planned the QENS experiment that was performed together with co-authors. I did the data analysis and wrote the dynamics part of the paper, and finalised the manuscript.

Table of Contents

Chapter 1

Introduction

The global CO_2 emissions have risen to a level where we have to make drastic changes in the society to limit the climate changes that are already ongoing on the planet. The emissions are distributed over all of our society and all sectors need to make a cut, however this is more straight forward in certain sectors. Figure 1.1 shows the greenhouse gas emissions in Europe 2017 presented by European Environment Agency [1]. A majority of the contributions come from the energy supply, industry and transport sectors where an electrification and green energy transition can provide a major reduction in greenhouse gas emissions. Green energy alternatives such as solar and wind power are increasing in popularity and decreasing in price [2].

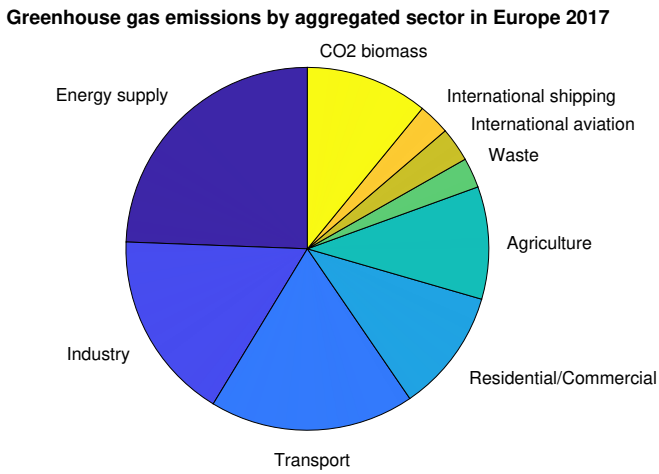

Figure 1.1: Greenhouse gas emissions by aggregated sector in Europe 2017.

However, one cannot escape the fact that these energy sources are weather and time dependent which means that efficient means for energy storage is needed for them to permanently replace fossil fuels [3]. Energy storage takes on different forms depending on the application, portable devices and electric vehicles are today dominated by the Lithium-ion battery (LIB) [4].

Since the commercialisation of LIBs in 1991 [5] they have been constantly under development, however, the electrolyte concept has basically been unchanged, being based on, $LiPF_6$ dissolved in carbonate solvents. Unfortunately these electrolytes are highly flammable and the salt decomposes into hazardous gases above 80°C [6], hence a safer electrolyte is preferred. To further develop the lithium ion battery an electrolyte that also allows for higher operating voltages is desired as it could increase the energy density. To achieve this, new electrolyte concepts are needed and several routes have been pursued, such as, polymer electrolytes [7], inorganic solid electrolytes [8, 9], highly concentrated electrolytes [10, 11] and ionic liquids [12]. This thesis focus on the two latter ones.

It has been shown that organic solvent electrolytes with high salt concentrations, 1-5 solvent molecules per lithium, have different electrochemical properties than those with lower salt concentrations [13–17]. These highly concentrated electrolytes, can be non-flammable, non volatile and have a large electrochemical stability window and makes for a good alternative to the conventional electrolyte. Despite the high salt concentration, and thereby a high viscosity, these electrolytes have a reasonable conductivity. This has been attributed to the large amount or charge carriers, but also potentially resulting from a conduction mechanism different from the vehicular transport in standard electrolytes as well as the development of a nanostructure not found in normal liquids [10]. For the development and possible use of these highly concentrated electrolytes it is important to understand the ion transport and the role of the local structure. Ionic liquids on the other hand are salts that are liquid at room temperature and are thereby constituted only of ions. Ionic liquids are in most cases non-flammable and can have large electrochemical stability windows [18], which makes them suitable as a replacement of the solvent in an electrolyte, or as an additive. Ionic liquids have also been studied for their peculiar structure. Unlike most liquids ILs show structuring on mesoscopic length scales [19–22]. This structure is believed to be an important factor for the dynamics in these systems.

This thesis focuses on understanding the structure and dynamics in ionic liquids and highly concentrated electrolytes. With experimental methods the dynamical processes in highly concentrated electrolytes have been investigated and identified on pico to nano second time scales on the mesoscopic length scale. Out of the different local processes not all contribute directly to the ion transport and to identify these have been an important part of the work. Temperature and salt concentration were used as variables as the local dynamics were investigated and the results were compared to the conductivity for further insight to the ion transport and relation between microscopic and macroscopic dynamics. For ionic liquids pressure was applied to add another control parameter, allowing for investigation of multiple state point in the PT-space that have the same macroscopic transport properties, i.e. conductivity. By keeping the conductivity constant while varying the temperature and pressure the motions that contribute to the conductivity were identified.

In this work small-angle X-ray scattering (SAXS) have been used to investigate the structure, while quasi-elastic neutron scattering (QENS) was used to study the local dynamics. The unique feature of QENS is that it probes the dynamics at relevant scales of time (1ps-10ns) and space (1-100Å) simultaneously. Thus, it covers the length scales of the nanostructures found in ionic liquids and HCEs. In the time scales investigated by QENS more than one process might take place, however, QENS provides tools to distinguish these from each other. The ion transport can then be separated from other processes, such as rotations of side chains.

Chapter 2

Electrolytes

In a battery the role of the electrolyte is to efficiently transport ions in between the anode and the cathode. This implies that a high ionic conductivity in the temperature range of the application is needed [23]. It is also essential that the electrolyte is non-conducting for electrons, so that they are forced to go through an external circuit rather than through the electrolyte to reach the opposite electrode. For lithium batteries liquid electrolytes are most common, it is then important that the electrolyte has a low enough viscosity to ensure wetting of the separator and electrodes in the cell and a wide working temperature range and low vapour pressure [24]. The electrolyte must of course also be both chemically and electrochemically stable in the voltage window used. On top of these properties the chemicals should be non toxic and from a commercially point of view cheap and abundant.Unfortunately there is so far no electrolyte that fulfils all these requirements and for each application a prioritisation of the properties has to be made to satisfy the most important criteria.

The typical liquid electrolyte consists of a solvent and a salt. The salt is essential for the ion transport and the solvents role is to dissolve the salt. For the choice of solvent the dielectric permittivity and viscosity is of particular importance. A high dielectric permittivity helps dissolving the salt while a low viscosity will facilitate fast ion transport. Usually two or more solvents need to be combined for the electrolyte to have both properties, as in the case of LP30, a commercially used electrolyte, where 1 M $LiPF_6$ is dissolved in equal parts of ethylene carbonate (EC) and dimethyl carbonate (DMC). EC has a high dielectric permittivity and creates a passivating layer on the interface between the anode and the electrolyte that prevents further decomposition of the electrolyte. EC is one of few, or possibly the only, organic solvent that can be used without co-intercalation into the graphite electrode taking place during cycling [25]. However, EC has a high melting point, around 36 °C [26], which makes it unsuitable for room temperature applications. The addition of DMC to the electrolyte lowers the melting point and the viscosity of the

solution making it high performing. To further tailor the properties to better fit the requirements of a particular application additives can be introduced to the electrolyte formulation [18].

Despite being one of the most popular commercial electrolytes on the market, there is still safety concerns associated with using LP30. The organic solvents are flammable and volatile and the salt is chemically unstable [27–29]. This calls for further research towards safe and highly performing electrolytes. Promising alternatives are highly concentrated electrolytes and ionic liquids [25,30], where the lack of free solvents, or in the case of ionic liquids the lack of solvents at all, provides conditions for safer electrolyte.

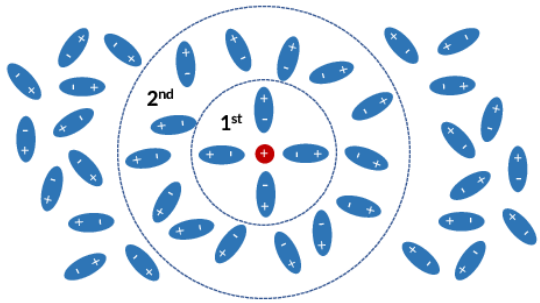

Figure 2.1: Schematic illustration of solvent molecules structured around a cation.

Many of the properties such as conductivity, safety and stability of an electrolyte as well as kinetics are related to the local electrolyte structure [31,32]. The local structure is of high importance to understand the properties and behaviour of the electrolyte. The local structure in the electrolyte is a result of the solvent molecules arranging themselves around the charged species. It is due to an electromagnetic dipole-moment in the otherwise neutral solvent molecules that interactions between the solvent and the anion and cation are possible. Figure 2.1 shows a schematic arrangement of solvent molecules around a cation. The small and symmetric shape of the cation results in a spherically symmetric electrical field, causing the solvent molecules nearby to align. This is referred to as the first solvation shell and is marked in the figure. Outside of the first solvation shell a second solvation shell is also found. Even though the strength of the field is heavily reduced as the distance from the ion

increases there is still some ordering. However, outside the second solvation shell the charge of the cation is screened and there is hardly any ordering left. This image of the local structure is only valid for low concentrations where the ions are properly separated.

The ion transport in electrolytes with a relatively low salt concentration is well described by a vehicular transport model [33]. In this scenario the ion moves along with its first solvation shell through the liquid. It can be approximated as a sphere moving in a viscous liquid and follows the Stokes-Einstein relation of the diffusion coefficient

$$D = \frac{k_b T}{6\pi r_s \eta} \tag{2.1}$$

where k_b is Boltzmann's constant, T is the temperature, r_s is the size of the solvation shell and η is the viscosity. However this is only valid for very dilute electrolytes where the interactions between ions are negligible [33], for higher concentrations the ion transport is more complex [34–36].

2.1 Highly concentrated electrolytes

The salt concentration of an electrolyte is often chosen as to maximise the conductivity and is in general around 1 mol/dm^3. Above this concentration the conductivity decreases as a result of a viscosity increase, therefore higher concentrations have previously not been considered as alternatives [10]. However, this changed when Yamada et al. showed that an electrolyte with a salt concentration of 3.2 mol/dm^3 LiTFSI in dimethyl sulfoxide, did not exhibit co-intercalation of the solvent into natural graphite [37]. They attribute the altered bulk property to a change in the solvation shell of the lithium-ions. Thus, at high salt concentration a different local structure is envisaged and as a result the properties of the electrolyte are changed. This enables the use of organic solvents that previously have been disregarded due to unfavourable properties, such as co-intercalation in graphite as in the case of dimethyl sulfoxide. Since then many highly concentrated systems have been investigated based on solvents such as propylene carbonate [38], acetonitrile [14], ethers [13], glymes [39] and water [40].

These highly concentrated electrolytes can be made safer than LP30 [10, 15, 39, 41, 42]. When designing the electrolyte there is a large number of

solvents and salts available to chose from. To ensure non-flammability a non-flammable solvent can simply be chosen. However, common non-flammable solvents have been found to have poor passivation ability of the electrode [25]. This on the other hand can be solved by choosing the right salt. It has been shown that as opposed to the electrolytes with low salt concentration where the solvent is making up the protective solid electrolyte interphase (SEI) at the electrode for highly concentrated electrolytes the SEI is to a large extent made up by anions [25]. The salt can then be chosen to create a good and stable SEI instead of using the chemically unstable salt $LiPF_6$ and the potential problems of using the non-flammable solvents is eliminated. Finally, in the highly concentrated electrolytes the volatility of the solvent is reduced due to the enhanced interactions between the cations and solvent molecules. [25]

Whereas the safety aspect might initially have been a driving force, highly concentrated electrolytes have shown several other advantages compared to conventional electrolytes. Yamada et al. showed with cycling experiments that a 4.5 M LiFSI/AN electrolyte was maintaining a higher capacity during fast charge and discharge of a natural graphite/lithium metal half cell compared to a cell with LP30 [14]. It is well known that the limitation of the charging rate of lithium ion batteries with a graphite electrode lies in the lithium intercalation kinetics. The fact that a highly concentrated electrolyte outperformed a conventional electrolyte points towards faster intercalation kinetics when using the HCE [14]. Moreover, the use of HCEs can help achieve higher energy density than state of the art batteries by expanding the voltage window of operation of the cell. Wang et al. [42] used a highly concentrated 5.5M LiFSI/DMC electrolyte to realise stable cycling of a 5V-class electrode as opposed to the 4V-class electrodes that are used with LP30 on the market today.

HCEs have also been investigated as electrolytes for next generation chemistries such as, Li-O_2, Na-O_2 and Li-S batteries. One of the major issues with Li-S cells is the dissolution of polysulfides in the electrolyte during cycling. However, highly concentrated electrolytes have been shown to prevent this dissolution. Since the solubility of a salt has a certain saturation degree for a given solvent and the polysulfides can be considered a salt, the highly concentrated electrolyte is already close to saturation before contact with the polysulfides and will inhibit the dissolution [43, 44]. Another issue for lithium-metal batteries, such as Li-S and Li-O_2, is dendrite formation on the lithium anode and there are reports of highly concentrated electrolytes addressing the problem. Qian et al. have reported suppression of dendrite growth for over 1000 cycles in a

Li-Cu cell in a 4M LiFSI/DME electorlyte [45].

However, there are some short comings of highly concentrated electrolytes. The large amount of salt needed increases the price of the electrolyte considerably. The second issue is that the high viscosity that comes with the high salt concentration causes problems with poor wettability of the separator and electrodes. [25] A suggested solution to the problem is to dilute the highly concentrated electrolyte with another solvent with low viscosity. This solvent should not interact with the solvation shells in order to keep the advantageous properties of the highly concentrated systems, while the viscosity is decreased [25]. This also lowers the amount of salt needed and hence reduces the price (provided that the price of the solvent is low).

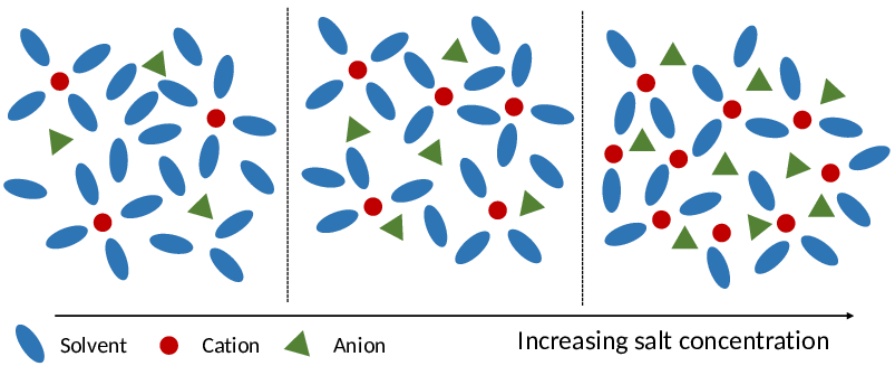

Figure 2.2: Local electrolyte structure as a function of concentration.

The development of HCE has to a large extent been empirically driven and in many respects a fundamental understanding of the local structures and dynamics is lacking. The change in physical and electrochemical properties has been suggested to be an effect of changes in the local structure [10]. Figure 2.2 shows a schematic of how the local structure changes with salt concentration. For low salt concentrations there are plenty of free solvent molecules and the first solvation shell of the cations consists of solvent molecules. As the salt concentration increases the anions will start to be a part of the first solvation shell and the number of free solvent molecules will decrease until a point where

there will be almost no free solvent molecules left in the electrolyte. There are a few experimental studies of the local structure performed with Raman spectroscopy that show that with increasing salt concentration the number of free solvent molecules are reduced to a limit where all solvent molecules are coordinated to a lithium ion [13, 14, 42, 46]. For the higher salt concentrations also the anion take part in the solvation shells with contact ion pairs (CIP) and aggregates (AGG) being formed. Yamada et al. reports that for 3.2 M of LiTFSI in DMSO, all TFSI anions and DMSO molecules are coordinated to lithium ions and forms a polymetric fluid network of Li^+ and TFSI [46].

2.1.1 Ion transport in HCEs

The ion transport of HCE differs from the conventional electrolytes where the vehicular ion transport is dominating. One proposed model of ion transport in HCEs is ligand exchange where the association and dissociation between the cation and the solvent molecules, or anions, is the fundamental process [35] rather than having the entire solvation shell moving as in vehicular transport [33]. Another model, that is described for highly concentrated aqueous electrolytes, is that the electrolyte undergoes phase separation into nanosized anion-rich domains, where the anions are rather immobile, and H_2O rich domains with cations dispersed [36]. Fast ion transport is then possible in domains through a vehicular mechanism in a network of H_2O. Based on results published the ion transport seems to be heavily dependent on the actual system.

Seo et al. published a study 2013 where they, through molecular dynamics simulations, investigated the dynamics in acetonitrile based electrolytes with varying salts and salt concentration [47]. They found that the anions stayed coordinated to lithium ions longer than the anions were coordinated to the solvent molecules. The anion-Li^+ residence time was found to vary with the different types of anions and for the TFSI-anion the residence time increased with the salt concentration, from 350 ps for 30AN:1LiTFSI up to 700 ps for 5AN:1LiTFSI. However, this trend was not seen for all salts. For the BF_4 anion a reversed behaviour was observed with shorter residence time for higher concentrations. Considerably shorter residence times were presented by Okoshi et al. for NaTFSI in DME and concentrations up to 40 mol% [35]. From molecular dynamics they found a life time of a solvation shell to be around 120 ps. A recent study by Åvall et at. present even shorter residence times [48]. By investigating the ligand exchange rates in PC and acetonitrile electrolytes

with concentrations of Li/$NaPF_6$ from 20:1 to 5:1 using ab initio molecular dynamics they have found residence times of 1-15 ps. A decrease in residence time was seen with concentration for both electrolytes in agreement with the trend for the BF_4 anion [47]. They also found that the Na-salt electrolytes show a shorter residence time than the lithium equivalents [48]. The interaction behaviour and residence times differ largely in studies for various molecules and it is at present not clear if the large difference comes from actual differences in the system or from different simulation techniques and definitions of when a molecule is in the solvation shell. Therefore, as always, it is important to verify the results with experiments.

One of few experimental studies of local dynamics in highly concentrated electrolytes was performed by Dokko et al [49]. From NMR measurements an unusually high lithium self-diffusion in a sulfolane based electrolyte was observed. This study showed that lithium diffused faster than both the anion and the solvent molecules. This contradicts the vehicular model, where the lithium is transported in a solvated form together with either anion and/or solvent molecules. They attributed this increased lithium diffusion to an additional jump diffusion [49], resulting in a mix of vehicular transport and jump diffusion. When looking at local dynamics experimentally another suitable tool is neutron scattering. With quasi-elastic neutron scattering one can access both the time and length scale of the motions of the ion transport and directly compare to MD simulations. However, to the best of our knowledge there are no published QENS-experiments on highly concentrated liquid electrolytes.

2.2 Ionic Liquids

Another highly concentrated system is ionic liquids, however, unlike previously discussed electrolytes ionic liquids consists only of ions i.e. there is no solvent involved. Ionic liquids are salts that are molten at relatively low temperatures [50]. The definition varies slightly and in literature one can also find definitions of ionic liquids as salts liquid below 100°C [51]. The low melting point of ionic liquids comes from the large size of the anions and cations. The size contributes to a charge delocalisation that together with asymmetry of the ions prevents efficient packing and therefore also crystallisation. There is a large amount of anions and cations suitable for ionic liquids and when designing an ionic liquid for a specific area of application there are many combinations to chose from in order to tailor the properties of the liquid [52].

Ionic liquids are good alternatives to organic solvents in electrolytes. First of all they are thermally stable and nonflammable which increases the safety aspect of the electrolyte [18]. On top of that they have a fairly high ionic conductivity, a large electrochemical stability window and are good solvents for many Li-salts [18]. Unfortunately there are also drawbacks, just like in the case of highly concentrated electrolytes, ionic liquids suffer from high viscosity as well as high cost [18]. A way to reduce both the price and the viscosity of ionic liquids is to mix them with low viscosity solvents [18]. Dilution can in the best case preserve the good properties of ionic liquid while handling the drawbacks.

As in the case of the highly concentrated electrolytes, the favourable properties of ionic liquids comes from the local structure. The absence of neutral molecules leaves us with only charged species that gives rise to charge ordering. This has been confirmed by, amongst others, Mackoy et al. in a MD simulation where the structure factor of 1-butyl-1-methylpyrrolidinium bis(trifluoromethylsulfonyl)imide (P14TFSI) showed two peaks [53]. The first peak, that is also found in simple liquids, represent the distance between molecules, a nearest neighbour distance of 4-5Å. The second peak was, with the help of partial structure factors, assigned to originate from the reoccurring distances between two anions or two cations of 7-8Å, hence there is a charge ordering with alternating charges found in ionic liquids that are not found in simple liquids. For ionic liquids with alkyl side chains with 6 carbons or more there will also be another ordering, seen from SAXS experiments [54]. The origin stems from the formation of apolar domains in the ionic liquid. These heterogeneities are around 20Å and originate from the segregation of the alkyl chains due to van der Waals interactions. Understanding the structure and dynamics on the local scale is thus of importance to understanding the ion transport in a potential electrolyte use.

Marzan and Boltoeva investigated interactions of an imidazolium based ionic liquid using NMR spectroscopy [55]. By varying the chain length n of the cation, $C_n$mim, they found that the longer the chain the slower self-diffusion. It was also found that the cation had a higher mobility than the TFSI-anion for chain lengths below 6, while above that the two ions had similar diffusion coefficients [55]. While changing the length of the alkyl chain the balance between coulombic forces, hydrogen bonding and van der Waals interactions is modified which gives rise to changes in the dynamics.

Dynamics in pure ionic liquids have been investigated rather thoroughly with QENS [56–60]. Kofu et al. investigated dynamics of imidazolium-based ionic liquids, with varying alkyl chain lengths and different anions as a function of temperature [57]. In this study they find three independent relaxations in the time scale of 1 ps to 10 ns. They claim these motions are, presented in order of falling relaxation time, ionic diffusion, in the shape of a jump diffusion, a relaxation of the imidazolium ring and an alkyl chain reorientation. These three motions are self-diffusive motions depending only on the ion itself. In another publication by the same authors [56], a motion of collective dynamics attributed to the heterogeneity in the structure is proposed. This motion is slower than all the self-diffusion processes. What is still lacking is a link between the macroscopic properties of the ionic liquid such as the conductivity and the local dynamics and structure of ionic liquids. This we have addressed in paper I and II in this thesis where we use a combination of dielectric spectroscopy and QENS.

Chapter 3

Methods

3.1 Dielectric spectroscopy

Dielectric spectroscopy is a useful method for characterising electrochemical systems where the dielectric properties of a material is measured as a function of frequency. The complex dielectric function, or dielectric permittivity ϵ^*, contains information about motions in a material. If time dependent motions, such as relaxations, conductivity or polarisation, take place the dielectric permittivity will have a time dependency [61].

One way of measuring the dielectric permittivity is via the electric impedance of the material. In an impedance experiment an alternating voltage is applied to a sample, see figure 3.1, and the resulting alternating current is measured. The impedance is then calculated using Ohms law. Equation 3.1 shows the relation between the current J, the voltage E, the Impedance Z and the dielectric permittivity,

$$\epsilon^*(\omega) = \frac{J^*(\omega)}{i\omega\epsilon_0 E^*(\omega)} = \frac{1}{i\omega Z^*(\omega) C_0} \tag{3.1}$$

where C_0 is the vacuum capacitance of the system [61], which is given by

$$C_0 = \epsilon_0 \frac{A}{d} \tag{3.2}$$

where A is the area of the electrodes in between which the material is placed and d is the distance between the electrodes.

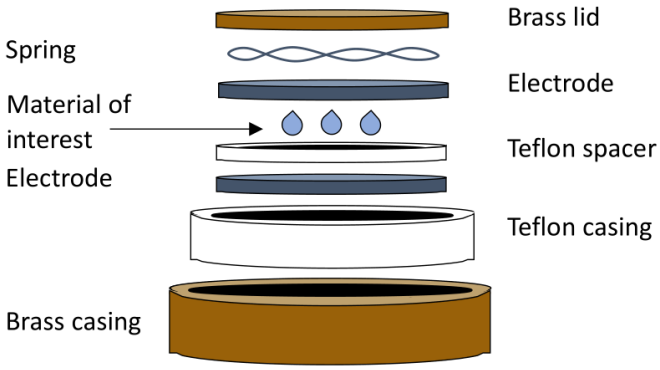

Figure 3.1: Sample cell setup for dielectric spectroscopy measurements.

The real part of the conductivity σ' of a material is related to the imaginary part of the permittivity as seen in equation 3.3 [62].

$$\epsilon^*(\omega) = \epsilon'(\omega) + i\epsilon''(\omega) = \epsilon'(\omega) + i\frac{\sigma'(\omega)}{\omega} \tag{3.3}$$

The DC-conductivity is the part of interest when investigating the conductivity of an electrolyte. It is found as the plateau in the curve of $\sigma'(\omega)$ seen in figure 3.2 [61].

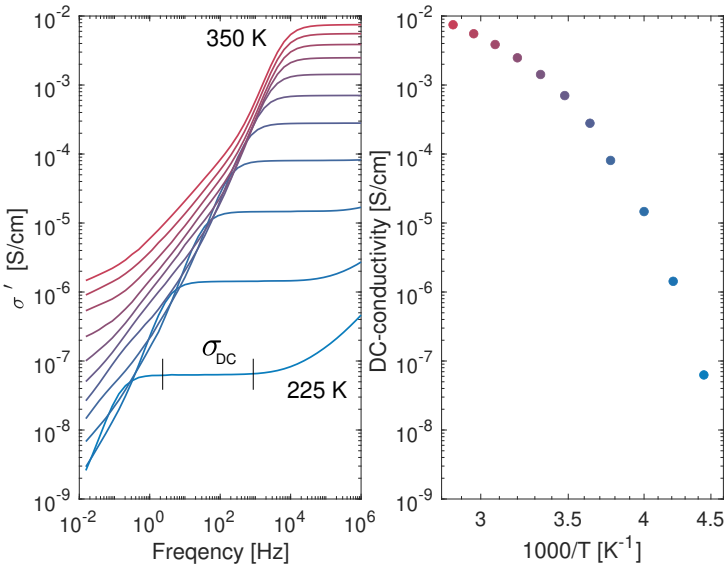

Figure 3.2: Left: Frequency dependent conductivity of a highly concentrated electrolyte in the temperature range 225-350 K. The DC-conductivity is found at the plateau as indicated in the figure and is shown in the figure to the right.

3.2 Small-Angle X-ray Scattering

Small-angle X-ray scattering is sensitive to changes in nano-scale electron density and can therefore be used to probe, for example, size distributions of nanoparticles, pore sizes or characteristic distances in partially ordered materials [63]. Figure 3.3 shows a schematic of a SAXS experiment. An incoming monochromatic X-ray beam with wavevector $\boldsymbol{k}_i$ is scattered off the sample in an angle of 2θ and the scattered intensity is registered by a detector. Equations 3.4 and 3.5 describe the wavevector $\boldsymbol{k}$ and the momentum transfer vector $\boldsymbol{Q}$.

$$|\boldsymbol{k}| = k = \frac{2\pi}{\lambda} \tag{3.4}$$

$$\boldsymbol{Q} = \boldsymbol{k}_s - \boldsymbol{k}_i \tag{3.5}$$

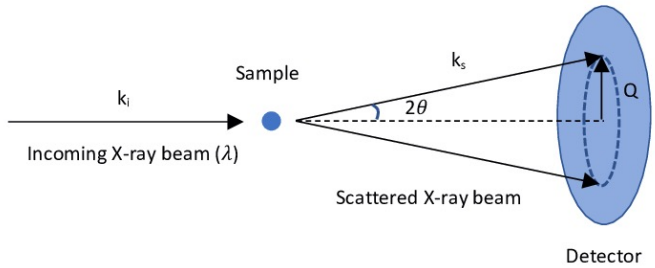

Figure 3.3: Schematic of a small-angle X-ray scattering experiment.

It is convenient to express the scattering pattern in terms of Q rather than 2θ since Q includes the information of λ so one can directly compare spectra from different instruments. $\boldsymbol{Q}$ can be related to ta real space distance through [64],

$$|\boldsymbol{Q}| \sim \frac{2\pi}{d} \tag{3.6}$$

and gives an idea of what length scale the features in the pattern originate from. For elastic scattering events the incoming and scattered wavevector have the same magnitude, $|\boldsymbol{k}_i| = |\boldsymbol{k}_s|$ and Q can be expressed in terms of θ as

$$|\boldsymbol{Q}| = Q = 4\pi \frac{\sin\theta}{\lambda}. \tag{3.7}$$

Figure 3.4a shows an example of a two dimensional SAXS pattern of an ionic liquid. The colorbar indicates the intensity of the signal i.e. the normalised number of photons registered by that part of the detector. For isotropic materials, such as liquids, the sample scatters equally in all azimuthal angles (marked as α in the figure) and the 2D pattern can be shown as a 1D pattern, I(Q), by integrating over all the azimuthal angles [65]. An example of such a curve is shown in figure 3.4b. In this SAXS pattern of an ionic liquid, we see two peaks, related to the presences of characteristic distances in the material, see further in section 2.2 on ionic liquids. From this type of data, we can determine if there is any type of order in the material, and on what length scales this order appears.

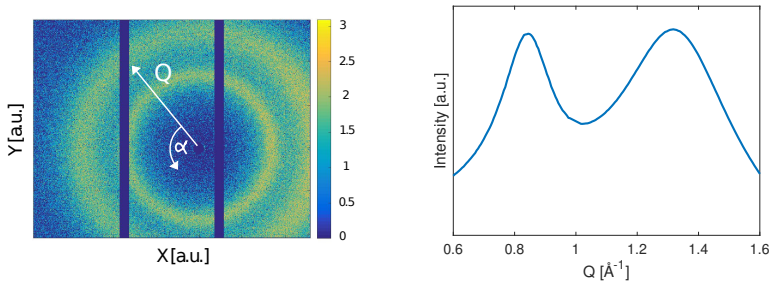

(a) (b)

Figure 3.4: Experimental SAXS data of P14TFSI in (a) two dimensions and (b) one dimension.

3.2.1 Instrumentation and data treatment

I22 is a small-angle scattering beamline at Diamond Light Source, Oxfordshire, United Kingdom and was used to investigate the structure of ionic liquids. There are many elements to take into account when setting up the instrument to suit a certain experiment, the geometry of the instrument, e.g. the incoming energy of the beam and the thickness of the sample. Assuming that the instrument geometry is fixed, that the sample and detector positions are locked, the angles 2θ that can be covered by the detectors are fixed. Looking back at equation 3.7, the only parameter left that affects the Q-range is the wavelength/energy of the incoming beam. The incoming energy of the beam at I22 can be varied from 6 to 20keV and can therefore be selected to fit the Q-range of interest of the sample studied.

What should also be taken into account is the sample thickness. The scattering intensity of a material increases linearly with the thickness, while the absorption increases exponentially. The resulting intensity is then given by

$$I \propto de^{-\mu d} \tag{3.8}$$

where d is the thickness of the sample and μ is the linear absorption coefficient [66]. The intensity function has a maximum transmission for d $=1/\mu$, thus the thickness should be chosen to match the linear absorption coefficient which is material specific and also energy dependent [64].

In order to separate the scattering from the sample from the contribution of

the sample cell and the background, a measurement of the empty cell is needed and is later subtracted from the signal. Before subtracting the empty cell and the background the scattered intensity is normalised. In front of the sample there is a monitor that measures the incoming intensity and after the sample there is a monitor to register the transmitted beam. Using these two intensities a normalisation can be done.

3.3 Quasi-Elastic Neutron Scattering

QENS is a tool to investigate dynamical processes on the typical time and length scales of atomic and molecular dynamics, making it suitable for investigations of for example proteins, polymers and ionic liquids [67]. In a neutron scattering experiment the neutron interacts with the nucleus of an atom. The strength of the interaction is determined by the scattering length, b. The scattering length depends on the particular nucleus and its spin state and since there is no theory to describe nuclear forces well enough to calculate the scattering lengths of nuclei, they are experimentally determined. The scattering length varies erratically over the periodic table and also between isotopes [68].

Quasi-elastic neutron scattering is an inelastic method where the energy exchange between the nucleus and the neutron is the sought after quantity. For elastic interactions equation 3.7 was used to express the momentum transfer, Q. For inelastic scattering $|\boldsymbol{k_i}| \neq |\boldsymbol{k_s}|$ and Q depends not only on the scattering angle but also on the energy change and is given by

$$Q = \sqrt{k_i^2 + k_s^2 - 2k_i k_s \cos(2\theta)}. \tag{3.9}$$

In a neutron scattering experiment the number of scattered neutrons per second in a solid angle $d\Omega$ with a final energy between E' and E'+dE' are measured and is described by the double differential scattering cross section

$$\frac{d^2\sigma}{d\Omega dE} = \frac{k_s}{k_i}\frac{1}{2\pi\hbar}\sum_{jj'}\overline{b_{j'}b_j}\int_{-\infty}^{\infty}\langle\exp(-i\boldsymbol{Q}\cdot\boldsymbol{R}_{j'}(0))\exp(i\boldsymbol{Q}\cdot\boldsymbol{R}_j(t))\rangle\exp(-i\omega t)dt, \tag{3.10}$$

where the index j and j′ run over all nuclei, $\boldsymbol{R_j}$ and $\boldsymbol{R}_{j'}$ are the position of nuclei j and j′ at the time t, $\langle\rangle$ denotes the thermal average and b is the

scattering length of the nucleus [68]. This expression describes the inter-particle correlations and their time evolution in terms of position operators of the particles of the scatterer. Under the assumption there is no correlation between the scattering length values, b, of different nuclei

$$\begin{aligned} \overline{b_{j'}b_j} &= (\overline{b})^2, \qquad j' \neq j, \\ \overline{b_{j'}b_j} &= \overline{b^2}, \qquad j' = j. \end{aligned} \tag{3.11}$$

equation 3.10 can then be expressed as

$$\begin{aligned} \frac{d^2\sigma}{d\Omega dE} &= \frac{k_s}{k_i}\frac{1}{2\pi\hbar}(\overline{b})^2 \sum_{jj'} \int_{-\infty}^{\infty} \langle \exp\left(-i\boldsymbol{Q}\cdot\boldsymbol{R}_{j'}(0)\right) \exp(i\boldsymbol{Q}\cdot\boldsymbol{R}_j(t))\rangle \exp(-i\omega t)dt \\ &+ \frac{k_s}{k_i}\frac{1}{2\pi\hbar}(\overline{b^2} - (\overline{b})^2) \sum_{j} \int_{-\infty}^{\infty} \langle \exp\left(-i\boldsymbol{Q}\cdot\boldsymbol{R}_{j}(0)\right) \exp(i\boldsymbol{Q}\cdot\boldsymbol{R}_j(t))\rangle \exp(-i\omega t)dt. \end{aligned} \tag{3.12}$$

The first term on the right hand side in equation 3.12 describes the coherent scattering. It depends on the correlation of both the same and different nuclei at different times. Hence, the coherent scattering gives information about the collective dynamics in a sample. The coherent cross section is expressed in terms of scattering length as

$$\sigma_{\text{coh}} = 4\pi(\overline{b})^2. \tag{3.13}$$

The second term on the right hand side in equation 3.12 is the incoherent scattering. Here the scattering depends on the correlation between the positions of the same nucleus at different times. Thus, the incoherent scattering gives information about self motion with the cross section

$$\sigma_{\text{inc}} = 4\pi(\overline{b^2} - (\overline{b})^2). \tag{3.14}$$

If the energy is expressed as $E = \hbar\omega$ and the expressions for the cross sections are used, equation 3.12 can be written as

$$\frac{d^2\sigma}{d\Omega\omega} = \frac{k_s}{k_i}\left(\frac{\sigma_{\text{coh}}}{4\pi}S_{\text{coh}}(Q,\omega) + \frac{\sigma_{\text{inc}}}{4\pi}S_{\text{inc}}(Q,\omega)\right). \tag{3.15}$$

where S_{coh} and S_{inc} are the structure factors. The coherent structure factor contain information about collective dynamics while the incoherent structure factor contain information about the self motion, e.g. self diffusion [67]. From equation 3.15 it can also be found that the cross sections σ_{coh} and σ_{inc} determine the amount of coherent and incoherent scattering. For samples with large

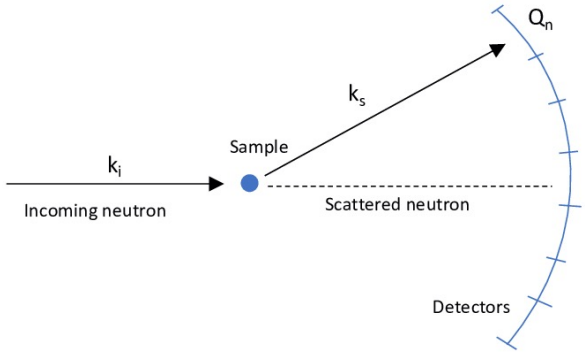

Figure 3.5: Schematic of a neutron scattering experiment

incoherent cross sections, like hydrogen rich materials, the incoherent scattering will dominate the signal. The cross section can be controlled to a certain extent by isotope substitution to increase or decrease the incoherent/coherent scattering to suit the purpose of the experiment.

In many cases the incoherent scattering is preferred in QENS experiments. This because models for incoherent scattering are well developed while there are few models for coherent scattering [69]. Hence, QENS is particularly useful for hydrogen rich materials that have strong incoherent signals. However, even though the incoherent signal is strong, it doesn't mean that the coherent signal is weak. This means that when the double differential cross section is measured in a QENS experiment and both the coherent and incoherent contribution is recorded the coherent scattering contribution can complicate the analysis [67]. Two methods can be used to handle this, either one chooses a sample where the incoherent signal is much larger than the coherent contribution by isotope substitution, or one uses polarised neutrons to separate the coherent and incoherent contributions [68].

A schematic of a QENS experiment is shown in figure 3.5. An incoming neutron is scattered by the sample and registered by one of several detectors. Each detector covers a certain angle, i.e. a certain q-value, and from the time-of-flight of the scattered neutron also the energy can be determined [67]. Thus, each detector measures the double differential cross section described in equation 3.10. Figure 3.6 shows an example of spectra of an acetonitrile based

highly concentrated electrolyte where the intensity is shown as a function of energy transfer. The broadening of the spectrum with respect to the resolution function reflects the dynamics in the material. An increased broadening is a result of faster relaxations, e.g. as a result of increasing temperature as shown in figure 3.6.

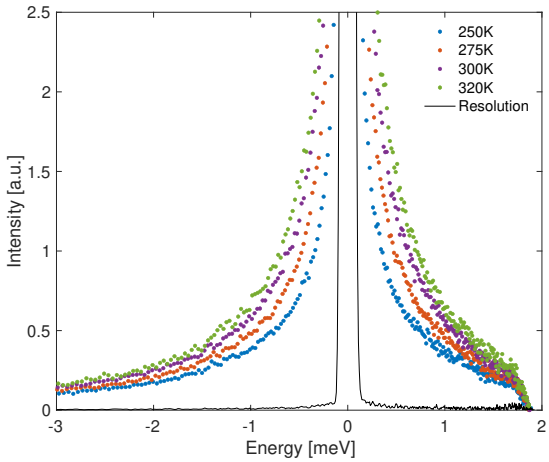

Figure 3.6: QENS spectra recorded at IN5 of LiTFSI in Acetonitrile (5AN:1LiTFSI) at Q=1.4$\mathring{A}^{-1}$ for different temperatures.

3.3.1 Experimental set up

The first thing to consider when planning a QENS experiment is what energy range and resolution is needed to investigate the motion of interest. For diffusion in electrolytes that typically takes place on the nanosecond scale a high energy resolution around 1 μeV is needed. If the motion of interest is fast, such as a relaxation of an alkyl chain on a molecule, a lower resolution, around 0.1 meV, could be considered. A higher energy resolution, implies that less neutrons of the incident beam will be used and therefore the signal will decrease. Not only should the instrument have the correct energy resolution, it also need to cover the relevant Q-range of the motions, typically in the range of 0.1-3 $\mathring{A}^{-1}$ [67].

The sample cell is preferably an annular cylindrical, if practically possible. A cylindrical geometry simplifies corrections related to absorption and multiple scattering. An alternative is to use a flat geometry that is more suitable for highly viscous samples and solids. However, for a flat geometry the contribution from the sample cell to the total signal will vary with the scattering angle and for highly absorbing materials the signal at angles parallel to the cell will be heavily reduced. The thickness of the sample is typically chosen to give 90% transmission, to minimise multiple scattering of the sample. The transmitted intensity a distance z into the material follows

$$I_z \propto e^{-\sigma n z} \tag{3.16}$$

where σ is the total cross section (scattering and absorption) and n is the number density [67], and the transmission T is

$$T = \frac{I_z}{I_0} = e^{-\sigma n z}. \tag{3.17}$$

For a 90% transmission we get the thickness as a function of scattering length and number density as

$$z = -\frac{\ln(0.9)}{\sigma n} \tag{3.18}$$

3.3.2 Data reduction

Several measurements in addition to the actual sample are needed to perform the data reduction, an empty cell measurement, a resolution measurement and a measurement of a purely elastically scatterer. Data reduction of neutron scattering data is highly dependent on the instrument and is in general performed with data treatment softwares, such as LAMP [70] and DAVE [71]. Initially all data has to be normalised to the incoming beam that is measured by a monitor placed in front of the sample. The signal from the empty cell can then be subtracted. The empty cell data should be recorded at the same temperature as the sample for a proper background subtraction. Self-shielding and self-absorption of the sample has to be taken into account and is calculated by the reduction softwares based on the sample cell geometry and density of the sample and its absorption and scattering cross sections. Vanadium is commonly used to calibrate the efficiency of the detectors since it is an isotropic scatterer. Finally a resolution measurement is needed. For resolution there are two options. Either a measurement of the sample at low temperature

where all motions in the sample are frozen or a measurement of vanadium or any other element that scatters purely elastically can be used.

3.3.3 Data analysis

For strong incoherent scatterers the dynamic structure factor S(Q,ω) can be approximated as

$$S(Q,\omega) \approx S_{\mathrm{inc}}(Q,\omega). \tag{3.19}$$

$S_{\mathrm{inc}}(Q,\omega)$ consists of both an elastic and an inelastic contribution. From the definition of the structure factor, the elastic contribution can be described by a delta function. The inelastic contribution in case of a simple exponential relaxation, such as free diffusion, is described by a Lorentzian function in frequency space. For multiple, in time well separated simple motions, the dynamical structure factor can be modelled as

$$S_{\mathrm{inc}(Q,\omega)} = A_0(Q)\delta(\omega) + \sum_i A_i L_i(Q,\omega), \tag{3.20}$$

where A_i is the area of the functions and the Lorentzian functions are described as

$$L_i(Q,\omega) = \frac{1}{\pi}\frac{\Gamma_i(Q)}{(\hbar\omega)^2 + \Gamma_i(Q)^2}. \tag{3.21}$$

where Γ is the half width at half maximum. This approach is valid for simple exponential relaxation processes that are independent and well separated in time, otherwise more complicated models are needed.

Figure 3.7 shows an example of QENS data, and fits to the data, of an acetonitrile electrolyte with the lithium salt LiTFSI at a concentration of 20ACN:1LiTFSI. The data was recorded at the Time-of-Flight spectrometer IN5 at ILL and is here visualised as the measured intensity for a specific Q-value as a function of energy. The data has been fitted with a resolution function, a linear background and two lorentzian functions. Thus, there are two relaxations in the sample at the investigated time scale (1-25ps). The information about the relaxations are found in the half width at half maximum (Γ) and the area of the lorentzian functions, further details are found in paper III.

The momentum transfer dependence of the width Γ provides information on what type of motion the relaxations corresponds to. For liquid samples three basic models are of relevance. The first model, equation 3.22, describes

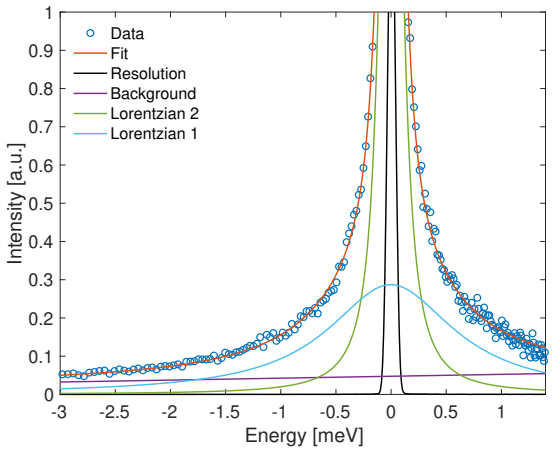

Figure 3.7: Fitted experimental QENS data of an ionic liquid. Two lorentzian functions are used to fit the experimental data, as well as a delta function and a linear background.

a Fickian diffusion where D is the diffusion constant. This is a continuous free diffusion and for small Q-values this model is valid for all diffusion processes [72],

$$\Gamma(Q) = \hbar D Q^2. \tag{3.22}$$

Two other models describe jump diffusion with different jump length distributions. The first, the Hall-Ross model [72], assumes a Gaussian distribution of the jump length and is described in equation 3.23 where l is the jump length and τ the residence time

$$\Gamma(Q) = \frac{\hbar}{\tau}\left(1 - \exp(-\frac{l^2 Q^2}{2})\right) \tag{3.23}$$

where

$$D = \frac{l^2}{2\tau}. \tag{3.24}$$

The second is the Singwi-Sjölander model [72], which assumes an exponential jump length distribution

$$\Gamma(Q) = \frac{\hbar}{\tau}\frac{(Ql)^2}{6 + (Ql)^2} \tag{3.25}$$

where

$$D = \frac{l^2}{6\tau}. \tag{3.26}$$

Figure 3.8 shows the momentum transfer dependence of the width for the different diffusion models for comparison. The Hall-Ross and Singwi-Sjölander models are plotted with a jump length l=1Å and a residence time τ=1ps and a simple diffusion is plotted with a diffusion coefficient of 1/3 Å^2/ps.

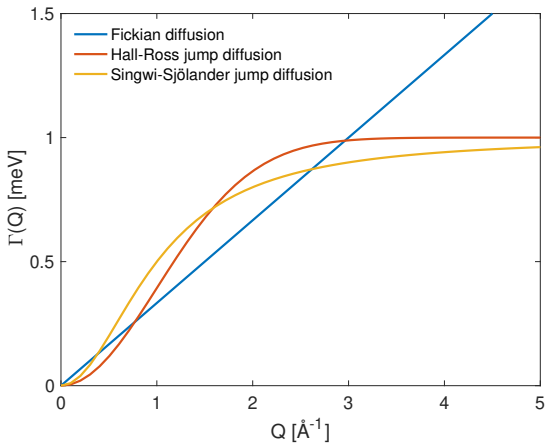

Figure 3.8: Diffusion models for Γ as a function of Q, where l was set to 1Å and τ to 1 ps for the jump diffusions and for the simple diffusion D was set to 1/3 Å^2/ps.

Figure 3.9 shows an example of Γ as a function of Q for a highly concentrated electrolyte with 2ACN:1LiTFSI where the data is fitted to a Singwi-Sjölander jump diffusion. The data was recorded at the backscattering spectrometer IN16B. From the fitting parameters it was concluded that the jump length was independent of temperature. However, the residence time show large temperature dependence, from 750 ps at 275K down to 50 ps at 350K see paper III for details.

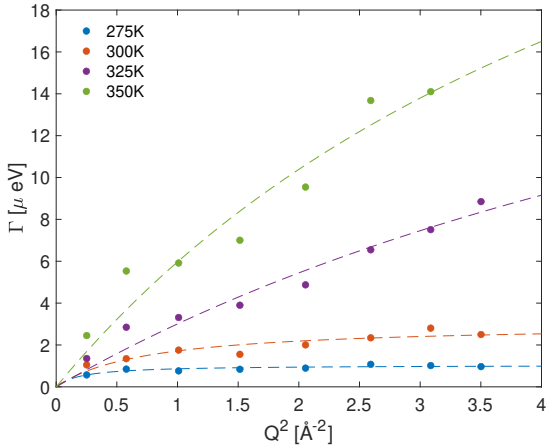

Figure 3.9: HWHM data fitted to a Singwi-Sjölander jump diffusion model for 2ACN:LiTFSI.

Local relaxations like chain rotations on molecules will show little to no Q dependence of Γ [57]. To access information of these motions the Elastic Incoherent Structure Factor (EISF) is an invaluable tool. It is defined as

$$EISF = \frac{A_{\text{elastic}}}{A_{\text{elastic}} + A_{\text{inelastic}}} \tag{3.27}$$

where A_{elastic} is the area of the elastic contribution and $A_{\text{inelastic}}$ is the area of the Lorentzian of interest. By fitting the EISF to different models one can determine what type of motion is observed and from the fitting parameters also learn about for example the geometry of the motion. Equation 3.28 describes the EISF for a methyl group rotation where j_0 is the zeroth order of the spherical Bessel function and d is the distance between the hydrogen and carbon atoms [72]. A is the fraction of signal that comes from the motion. For a hydrogen rich molecule it can be approximated to the ratio of hydrogen atoms taking part in the motion. For a methyl group rotation this corresponds to 3 so A will be 3 divided by the total number of hydrogen atoms of the molecule.

$$EISF_{\text{Methyl rotation}} = (1 - A) + A\frac{1}{3}\left[1 + 2j_0\left(\sqrt{\frac{8}{3}}Qd\right)\right] \tag{3.28}$$

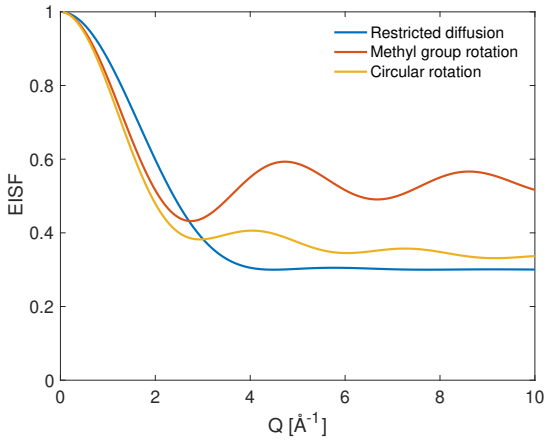

Figure 3.10: EISF for different models, where A=0.7 and r=d=1.

Another useful model is

$$EISF_{\text{Circular rotation}} = (1 - A) + A\frac{1}{N}\sum_{n=1}^{N} j_0\left[2Qr\sin\left(\frac{n\pi}{N}\right)\right] \tag{3.29}$$

that describes a random jumps on a circle of radius r with N equivalent sites [72]. For large values of N it corresponds to a continuous rotational diffusion and can be used to model the motions of alkyl chains. A third model describes a restricted diffusion inside a sphere of radius r [72].

$$EISF_{\text{Restricted diffusion}} = (1 - A) + A\left[\frac{3j_1(Qr)}{Qr}\right]^2 \tag{3.30}$$

Figure 3.10 show examples of the EISF for the presented models. A value of A=0.7 was used and r=d=1. In figure 3.11 the EISF was used to identify a local relaxation in an ionic liquid as a function of pressure measured at IN5, ILL. The data has been fitted to a restricted diffusion according to 3.30. From the fitting parameters a radius of the motion of around 1.3 Å was extracted. This motion is believed to be a librational relaxation of the carbon ring in the cation, see paper II for details.

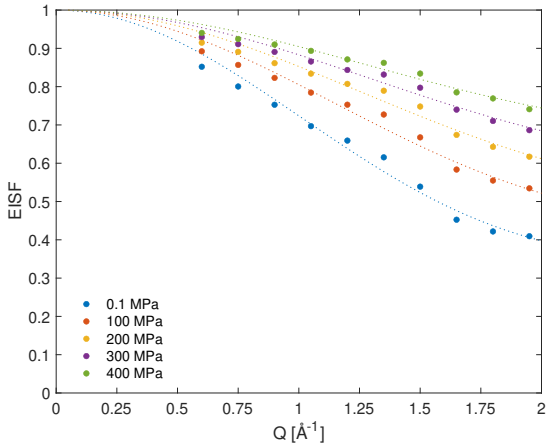

Figure 3.11: EISF for an ionic liquid as a function of pressure fitted to a restricted diffusion.

In an actual experiment the measured signal will also have a contribution of the resolution of the instrument and a background need to be taken into account [73],

$$S_{\text{measured}}(Q,\omega) = (S_{\text{inc}}(Q,\omega) \otimes R(Q,\omega)) + BG \tag{3.31}$$

where R(Q,ω) is the resolution function of the instrument and $\otimes$ is the convolution operator and BG is background.

Chapter 4

Results

4.1 Structure in highly concentrated systems

The nanostructure of ionic liquids is revealed by two peaks in the structure factor. The molecular peak corresponding to the nearest neighbour distance, and the charge ordering peak, that arises from the reappearing anion-anion and cation-cation distance [74]. Depending on the length of the alkyl chains of the cation also a third ordering can be found, corresponding to the formation of apolar domains [54]. For the material investigated in our study, P14TFSI, the alkyl chain is too short for the third peak to be seen and therefore only information about the charge ordering can be obtained. As temperature and pressure were applied to the sample, an expansion and compression occurred respectively, seen as shifts in the peak positions. To take this study one step further, we investigated the structure for temperature and pressure state points that have the same macroscopic conductivity. The structure was found to be more or less constant at these P,T points for the nearest neighbour distances, while the charge ordering peak showed some deviations. The invariance suggests a strong connection between the local structure on the nearest neighbour length scales and the dynamics.

Pure acetonitrile has only one broader peak in the structure factor, the nearest neighbour peak, figure 4.1. From fitting of the peak it is evident that it is in fact two close adjacent peaks corresponding to parallel and anti-parallel nearest neighbour ordering of the acetonitrile molecules. As salt is added, a second peak appears at lower Q-values and increases in intensity with salt concentration. This peak occurs around the same position as the charge ordering peak for ionic liquids, see comparison in figure 4.1. We believe that the origin of the peak arises from correlations between solvated Li-ions and the formation of aggregates.

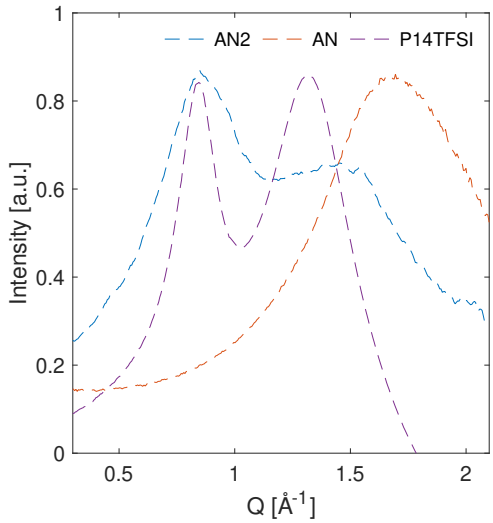

Figure 4.1: SAXS patterns of acetonitrile, a highly concentrated acetonitrile electrolyte and an ionic liquid.

4.2 Probing dynamics with neutron scattering

Local dynamics of an ionic liquid, P14TFSI, were investigated through a combination of two QENS instruments to cover a large time window, figure 4.2. With IN5 faster dynamics can be investigated, typically local dynamics of the molecule like alkyl chain rotations or librational motions. IN16B is an instrument with higher energy resolution, and therefore measures slower dynamics e.g. diffusional motions.

The investigated ionic liquid shows dynamics in both time windows. In the the window of faster dynamics, two processes are found. The lack of a Q-dependence in the HWHM indicates that these motions are of a local origin [57]. Fitting of the data indicates that one of the processes is a librational motion of the carbon ring of the cation. The other motion is believed to be a circular rotation of the butyl chain of the cation. These motions show little to no temperature dependence and are therefore believed to separated from the conductivity. The IN16B data reveals a confined translational diffusion

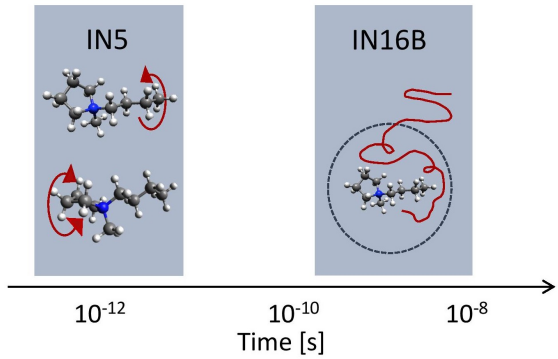

Figure 4.2: Time scales covered by the QENS instruments IN5 and IN16B and examples of motions that typically occur on these time scales.

process. The confinement is believed to be about 4-5Å and corresponds well to the charge ordering in the liquid. The size of the confinement increases with temperature and decreases with pressure, which is also seen from the SAXS-studies of the structure. For temperature and pressure points with constant conductivity the size of the confinement is found to be invariant, this is also the case for the diffusion coefficients. From these results it could be assumed that the conductivity is controlled by this confined translational diffusion.

Acetonitrile based electrolytes with varying concentrations of LiTFSI, were studied using QENS on IN16B. The dynamics in the sample were found to slow down with increasing salt concentration to an extent that only the high concentrations, 5 ACN:1 LiTFSI and 2 ACN: 1 LiTFSI, were in the time window of the instrument. On the same time scale as for the ionic liquid, the highly concentrated electrolytes show diffusional motions. This particular motion was fitted to a jump diffusion where the jump length was found to be invariant of temperature and concentration, see figure 4.3. The residence time in between jumps, however, was found to be highly dependent on temperature and concentration where high temperatures showed a shorter residence time, and the higher concentrations a longer residence time.

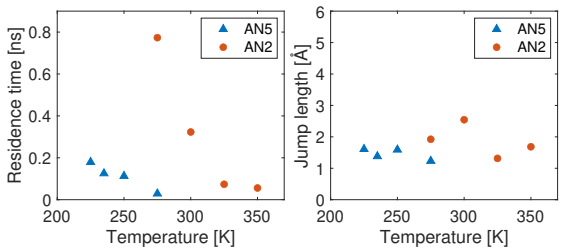

Figure 4.3: Residence time and jump length found in acetonitrile based highly concentrated electrolytes.

4.3 Pressure effect on ionic liquids

Ionic liquids are fundamentally interesting systems with an ordering on the mesoscopic length scale that arise from competing Coulomb and van der Waals interactions [75]. To learn more about the systems and the interactions, pressure was applied to disturb the system. With the help of pressure and temperature the density of the system was altered all while looking at the structure and dynamics of the IL. Scaling the dynamics with the density, showed that the charge transport, microscopic alpha relaxation, phonon dynamics, viscosity and self diffusion all scale with the same scaling variable. This scaling variable is intermediate of that of van der Waals bonding liquids and hydrogen bonding liquids [76–79]. While ionic interactions are of higher energy than hydrogen bonds, it is surprising that the scaling ends up in between the hydrogen and van der Waals bonding liquids, and in fact slightly leaning towards the van der Waals liquids. One could therefore argue that it is the van der Waals interactions that controls the dynamics rather than the ionic interactions in these liquids. A possible explanation to this is that the charges are efficiently screened in the ionic liquid, hence, the dynamics are dominated by the van der Waals interactions.

Chapter 5

Outlook

Fundamental studies of the structure and dynamics of ionic liquids and highly concentrated electrolytes, as presented in this thesis, are of importance to understand the behaviours of these systems and their properties in order to fully take advantage of their potential. However, for commercially viable applications the cost and viscosity are too high for both ILs and HCEs and future research should target these issues. Dilution of the HCEs and ILs can lower both the cost and the viscosity while maintaining the advantageous properties of these systems. As the systems are diluted the local structures and dynamics will change, and studies are needed to understand how it changes in order to design better electrolytes. A combination of experimental techniques such as Raman, SAXS, NMR and QENS with simulations would be to recommend for this since neither of the techniques alone can provide the full picture.

Acknowledgements

Thank you...

- Aleksandar for believing that I can do this, even though I have doubted it many times. Thank you for your patience, positive energy and magic ability to make even mediocre things sound really good.
- Marianne for your great support, scientifically but mostly morally. I miss you (and your chocolate).
- Past and present member of (K)MF. You really make the work worth it. During this spring that I have spent mostly working from home it really has been evident how much better work is together with you. A special thank you to my PhD-twin Matthew who has been with me on this journey since the first day. Thank you my awesome office mates Linnea and Adrián for making ours the best office! Thank you Gustav and Simon for always having time for scientific questions, gossip and quizzes. I miss having you around.
- SwedNess for funding my research and providing me with courses, visits and a great group of colleagues and friends. Thank you to Elin and Karolina (also known as Willy & Rudy) for always making me laugh.
- Family for always being there in thick and thin and for providing the best group calls in the world.
- Andreas, the love of my life. Thank you for helping me when my Matlab code is not running, for being a great office mate during the spring and for always supporting me. ♡

Bibliography

[1] European Environment Agency. Greenhouse gas emissions by aggregated sector. https://www.eea.europa.eu/data-and-maps/indicators/greenhouse-gas-emission-trends-6/assessment-3, December 2019.

[2] International Renewable Energy Agency. Renewable power generation costs in 2018. https://www.irena.org/publications/2019/May/Renewable-power-generation-costs-in-2018, May 2019.

[3] Guido Pleßmann, Matthias Erdmann, Markus Hlusiak, and Christian Breyer. Global Energy Storage Demand for a 100% Renewable Electricity Supply. *Energy Procedia*, 46:22–31, 2014.

[4] 1 - Rechargeable lithium batteries: key scientific and technological challenges. In Alejandro A B T Rechargeable Lithium Batteries Franco, editor, *Woodhead Publishing Series in Energy*, pages 1–17. Woodhead Publishing, 2015.

[5] T Nagaura and K Tozawa. Progress in batteries and solar cells. *JEC Press*, 9:209, 1990.

[6] Amer Hammami, Nathalie Raymond, and Michel Armand. Lithium-ion batteries: runaway risk of forming toxic compounds. *Nature*, 424(6949):635–636, aug 2003.

[7] Daniel T Hallinan and Nitash P Balsara. Polymer Electrolytes. *Annual Review of Materials Research*, 43(1):503–525, jul 2013.

[8] Arumugam Manthiram, Xingwen Yu, and Shaofei Wang. Lithium battery chemistries enabled by solid-state electrolytes. *Nature Reviews Materials*, 2(4):16103, 2017.

[9] Jürgen Janek and Wolfgang Zeier. A solid future for battery development. *Nature Energy*, 1:16141, sep 2016.

[10] Yuki Yamada and Atsuo Yamada. Review—superconcentrated electrolytes for lithium batteries. *Journal of The Electrochemical Society*, 162(14):A2406–A2423, 2015.

[11] Jianming Zheng, Joshua A Lochala, Alexander Kwok, Zhiqun Daniel Deng, and Jie Xiao. Research Progress towards Understanding the Unique Interfaces between Concentrated Electrolytes and Electrodes for Energy Storage Applications. *Advanced Science*, 4(8):1700032, aug 2017.

[12] Masayoshi Watanabe, Morgan L Thomas, Shiguo Zhang, Kazuhide Ueno, Tomohiro Yasuda, and Kaoru Dokko. Application of Ionic Liquids to Energy Storage and Conversion Materials and Devices. *Chemical Reviews*, 117(10):7190–7239, may 2017.

[13] Yuki Yamada, Makoto Yaegashi, Takeshi Abe, and Atsuo Yamada. A superconcentrated ether electrolyte for fast-charging Li-ion batteries. *Chemical Communications*, 49(95):11194–11196, 2013.

[14] Yuki Yamada, Keizo Furukawa, Keitaro Sodeyama, Keisuke Kikuchi, Makoto Yaegashi, Yoshitaka Tateyama, and Atsuo Yamada. Unusual Stability of Acetonitrile-Based Superconcentrated Electrolytes for Fast-Charging Lithium-Ion Batteries. *Journal of the American Chemical Society*, 136(13):5039–5046, apr 2014.

[15] Kazuhide Ueno, Kazuki Yoshida, Mizuho Tsuchiya, Naoki Tachikawa, Kaoru Dokko, and Masayoshi Watanabe. Glyme–Lithium Salt Equimolar Molten Mixtures: Concentrated Solutions or Solvate Ionic Liquids? *The Journal of Physical Chemistry B*, 116(36):11323–11331, sep 2012.

[16] Shiro Seki, Nobuyuki Serizawa, Katsuhito Takei, Kaoru Dokko, and Masayoshi Watanabe. Charge/discharge performances of glyme–lithium salt equimolar complex electrolyte for lithium secondary batteries. *Journal of Power Sources*, 243:323–327, 2013.

[17] Mengyun Nie, Daniel P Abraham, Daniel M Seo, Yanjing Chen, Arijit Bose, and Brett L Lucht. Role of Solution Structure in Solid Electrolyte Interphase Formation on Graphite with LiPF6 in Propylene Carbonate. *The Journal of Physical Chemistry C*, 117(48):25381–25389, dec 2013.

[18] Johan Scheers, Sébastien Fantini, and Patrik Johansson. A review of electrolytes for lithium–sulphur batteries. *Journal of Power Sources*, 255:204–218, 2014.

[19] Alessandro Triolo, Andrea Mandanici, Olga Russina, Virginia Rodriguez-Mora, Maria Cutroni, Christopher Hardacre, Mark Nieuwenhuyzen, Hans-Jurgen Bleif, Lukas Keller, and Miguel Angel Ramos. Thermodynamics,

Structure, and Dynamics in Room Temperature Ionic Liquids: The Case of 1-Butyl-3-methyl Imidazolium Hexafluorophosphate ([bmim][PF6]). *The Journal of Physical Chemistry B*, 110(42):21357–21364, 2006.

[20] Nicholas A. Mauro Allison M. Fleshman. Temperature-dependent structure and transport of ionic liquids with short-and intermediate-chain length pyrrolidinium cations. *Journal of Molecular Liquids*, 279:23–31, 2019.

[21] Yukihiro Yoshimura, Takahiro Takekiyo, Yoshihiro Koyama, Mayumi Takaku, Misaho Yamamura, Natsumi Kikuchi, Daisuke Wakabayashi, Nobumasa Funamori, Kiyoto Matsuishi, Hiroshi Abe, and Nozomu Hamaya. High-pressure glass formation of a series of 1-alkyl-3-methylimidazolium bis(trifluoromethanesulfonyl)imide homologues. *Phys. Chem. Chem. Phys.*, 20(1):199–205, 2018.

[22] Kartik Pilar, Victor Balédent, Mehdi Zeghal, Patrick Judeinstein, Sangsik Jeong, Stefano Passerini, and Steve Greenbaum. Communication: Investigation of ion aggregation in ionic liquids and their solutions with lithium salt under high pressure. *The Journal of Chemical Physics*, 148(3):31102, 2018.

[23] John B. Goodenough and Youngsik Kim. Challenges for rechargeable li batteries. *Chemistry of Materials*, 22(3):587–603, 2010.

[24] Y. Wu. *Lithium-Ion Batteries: Fundamentals and Applications*. Electrochemical Energy Storage and Conversion. CRC Press, 2015.

[25] Yuki Yamada, Jianhui Wang, Seongjae Ko, Eriko Watanabe, and Atsuo Yamada. Advances and issues in developing salt-concentrated battery electrolytes. *Nature Energy*, 4(4):269–280, 2019.

[26] Kang Xu. Nonaqueous Liquid Electrolytes for Lithium-Based Rechargeable Batteries. *Chemical Reviews*, 104(10):4303–4418, oct 2004.

[27] Catia Arbizzani, Giulio Gabrielli, and Marina Mastragostino. Thermal stability and flammability of electrolytes for lithium-ion batteries. *Journal of Power Sources*, 196(10):4801–4805, 2011.

[28] Tetsuya Kawamura, Arihisa Kimura, Minato Egashira, Shigeto Okada, and Jun-Ichi Yamaki. Thermal stability of alkyl carbonate mixed-solvent electrolytes for lithium ion cells. *Journal of Power Sources*, 104(2):260–264, 2002.

[29] Gerardine G Botte, Ralph E White, and Zhengming Zhang. Thermal stability of LiPF6–EC:EMC electrolyte for lithium ion batteries. *Journal of Power Sources*, 97-98:570–575, 2001.

[30] K Karuppasamy, Jayaraman Theerthagiri, Dhanasekaran Vikraman, Chang-Joo Yim, Sajjad Hussain, Ramakant Sharma, Thandavaryan Maiyalagan, Jiaqian Qin, and Hyun-Seok Kim. Ionic Liquid-Based Electrolytes for Energy Storage Devices: A Brief Review on Their Limits and Applications. *Polymers*, 12(4):918, apr 2020.

[31] Kang Xu, Yiufai Lam, Sheng S Zhang, T Richard Jow, and Timothy B Curtis. Solvation Sheath of Li+ in Nonaqueous Electrolytes and Its Implication of Graphite/Electrolyte Interface Chemistry. *The Journal of Physical Chemistry C*, 111(20):7411–7421, may 2007.

[32] Kang Xu. "charge-transfer" process at graphite/electrolyte interface and the solvation sheath structure of li+ in nonaqueous electrolytes. *Journal of The Electrochemical Society*, 154(3):A162, 2007.

[33] Yuichi Aihara, Kyoko Sugimoto, William S Price, and Kikuko Hayamizu. Ionic conduction and self-diffusion near infinitesimal concentration in lithium salt-organic solvent electrolytes. *The Journal of Chemical Physics*, 113(5):1981–1991, jul 2000.

[34] Zhen-Kun Tang, John S Tse, and Li-Min Liu. Unusual Li-Ion Transfer Mechanism in Liquid Electrolytes: A First-Principles Study. *The Journal of Physical Chemistry Letters*, 7(22):4795–4801, nov 2016.

[35] Masaki Okoshi, Chien-Pin Chou, and Hiromi Nakai. Theoretical Analysis of Carrier Ion Diffusion in Superconcentrated Electrolyte Solutions for Sodium-Ion Batteries. *The Journal of Physical Chemistry B*, 122(9):2600–2609, mar 2018.

[36] Oleg Borodin, Liumin Suo, Mallory Gobet, Xiaoming Ren, Fei Wang, Antonio Faraone, Jing Peng, Marco Olguin, Marshall Schroeder, Michael S Ding, Eric Gobrogge, Arthur von Wald Cresce, Stephen Munoz, Joseph A Dura, Steve Greenbaum, Chunsheng Wang, and Kang Xu. Liquid Structure with Nano-Heterogeneity Promotes Cationic Transport in Concentrated Electrolytes. *ACS Nano*, 11(10):10462–10471, oct 2017.

[37] Yuki Yamada, Yasuyuki Takazawa, Kohei Miyazaki, and Takeshi Abe. Electrochemical Lithium Intercalation into Graphite in Dimethyl Sulfoxide-

Based Electrolytes: Effect of Solvation Structure of Lithium Ion. *The Journal of Physical Chemistry C*, 114(26):11680–11685, jul 2010.

[38] Soon-Ki Jeong, Hee-Young Seo, Dong-Hak Kim, Hyun-Kak Han, Jin-Gul Kim, Yoon Bae Lee, Yasutoshi Iriyama, Takeshi Abe, and Zempachi Ogumi. Suppression of dendritic lithium formation by using concentrated electrolyte solutions. *Electrochemistry Communications*, 10(4):635–638, 2008.

[39] Kazuki Yoshida, Mizuho Tsuchiya, Naoki Tachikawa, Kaoru Dokko, and Masayoshi Watanabe. Change from Glyme Solutions to Quasi-ionic Liquids for Binary Mixtures Consisting of Lithium Bis(trifluoromethanesulfonyl)amide and Glymes. *The Journal of Physical Chemistry C*, 115(37):18384–18394, sep 2011.

[40] Liumin Suo, Oleg Borodin, Tao Gao, Marco Olguin, Janet Ho, Xiulin Fan, Chao Luo, Chunsheng Wang, and Kang Xu. "Water-in-salt" electrolyte enables high-voltage aqueous lithium-ion chemistries. *Science*, 350(6263):938 LP – 943, nov 2015.

[41] Dennis W. McOwen, Daniel M. Seo, Oleg Borodin, Jenel Vatamanu, Paul D. Boyle, and Wesley A. Henderson. Concentrated electrolytes: decrypting electrolyte properties and reassessing al corrosion mechanisms. *Energy Environ. Sci.*, 7:416–426, 2014.

[42] Jianhui Wang, Yuki Yamada, Keitaro Sodeyama, Ching Hua Chiang, Yoshitaka Tateyama, and Atsuo Yamada. Superconcentrated electrolytes for a high-voltage lithium-ion battery. *Nature Communications*, 7(1):12032, 2016.

[43] Liumin Suo, Yong-Sheng Hu, Hong Li, Michel Armand, and Liquan Chen. A new class of Solvent-in-Salt electrolyte for high-energy rechargeable metallic lithium batteries. *Nature Communications*, 4(1):1481, 2013.

[44] Kaoru Dokko, Naoki Tachikawa, Kento Yamauchi, Mizuho Tsuchiya, Azusa Yamazaki, Eriko Takashima, Jun-Woo Park, Kazuhide Ueno, Shiro Seki, and Nobuyuki Serizawa. Solvate ionic liquid electrolyte for li-s batteries. *Journal of the Electrochemical Society*, 160(8):A1304–A1310, January 2013.

[45] Jiangfeng Qian, Wesley A Henderson, Wu Xu, Priyanka Bhattacharya, Mark Engelhard, Oleg Borodin, and Ji-Guang Zhang. High rate and

stable cycling of lithium metal anode. *Nature Communications*, 6(1):6362, 2015.

[46] Yuki Yamada, Kenji Usui, Ching Hua Chiang, Keisuke Kikuchi, Keizo Furukawa, and Atsuo Yamada. General observation of lithium intercalation into graphite in ethylene-carbonate-free superconcentrated electrolytes. *ACS Applied Materials & Interfaces*, 6(14):10892–10899, 2014. PMID: 24670260.

[47] Daniel M Seo, Oleg Borodin, Daniel Balogh, Michael O'Connell, Quang Ly, Sang-Don Han, Stefano Passerini, and Wesley A Henderson. Electrolyte Solvation and Ionic Association III. Acetonitrile-Lithium Salt Mixtures–Transport Properties. *Journal of The Electrochemical Society*, 160(8):A1061–A1070, 2013.

[48] Gustav Åvall and Patrik Johansson. A novel approach to ligand-exchange rates applied to lithium-ion battery and sodium-ion battery electrolytes. *The Journal of chemical physics*, 152(23):234104, jun 2020.

[49] Kaoru Dokko, Daiki Watanabe, Yosuke Ugata, Morgan L Thomas, Seiji Tsuzuki, Wataru Shinoda, Kei Hashimoto, Kazuhide Ueno, Yasuhiro Umebayashi, and Masayoshi Watanabe. Direct Evidence for Li Ion Hopping Conduction in Highly Concentrated Sulfolane-Based Liquid Electrolytes. *The Journal of Physical Chemistry B*, 122(47):10736–10745, nov 2018.

[50] G B Appetecchi, M Montanino, and S Passerini. Ionic Liquid-Based Electrolytes for High Energy, Safer Lithium Batteries. In *Ionic Liquids: Science and Applications*, volume 1117 of *ACS Symposium Series*, pages 4–67. American Chemical Society, jan 2012.

[51] K. Ghandi. A Review of Ionic Liquids, Their Limits and Applications. *Green and Sustainable Chemistry*, 4(1):44–53, 2014.

[52] Erlendur Jónsson. Ionic liquids as electrolytes for energy storage applications – A modelling perspective. *Energy Storage Materials*, 25:827–835, 2020.

[53] Travis Mackoy, Nicholas A Mauro, and Ralph A Wheeler. Temperature Dependence of Static Structure Factor Peak Intensities for a Pyrrolidinium-Based Ionic Liquid. *The Journal of Physical Chemistry B*, 123(7):1672–1678, feb 2019.

[54] Luis Aguilera, Johannes Völkner, Ana Labrador, and Aleksandar Matic. The effect of lithium salt doping on the nanostructure of ionic liquids. *Phys. Chem. Chem. Phys.*, 17(40):27082–27087, 2015.

[55] Valérie Mazan and Maria Boltoeva. Insight into the ionic interactions in neat ionic liquids by Diffusion Ordered Spectroscopy Nuclear Magnetic Resonance. *Journal of Molecular Liquids*, 240:74–79, 2017.

[56] Maiko Kofu, Michihiro Nagao, Takeshi Ueki, Yuzo Kitazawa, Yutaro Nakamura, Syota Sawamura, Masayoshi Watanabe, and Osamu Yamamuro. Heterogeneous Slow Dynamics of Imidazolium-Based Ionic Liquids Studied by Neutron Spin Echo. *The Journal of Physical Chemistry B*, 117(9):2773–2781, mar 2013.

[57] Maiko Kofu, Madhusudan Tyagi, Yasuhiro Inamura, Kyoko Miyazaki, and Osamu Yamamuro. Quasielastic neutron scattering studies on glass-forming ionic liquids with imidazolium cations. *The Journal of Chemical Physics*, 143(23):234502, 2015.

[58] Fumiya Nemoto, Maiko Kofu, Michihiro Nagao, Kazuki Ohishi, Shin-ichi Takata, Jun-ichi Suzuki, Takeshi Yamada, Kaoru Shibata, Takeshi Ueki, Yuzo Kitazawa, Masayoshi Watanabe, and Osamu Yamamuro. Neutron scattering studies on short- and long-range layer structures and related dynamics in imidazolium-based ionic liquids. *The Journal of Chemical Physics*, 149(5):54502, 2018.

[59] Miguel A González, Bachir Aoun, David L Price, Zunbeltz Izaola, Margarita Russina, Jacques Ollivier, and Marie-Louise Saboungi. Molecular dynamics in 1-alkyl-3-methylimidazolium bromide ionic liquids: A reanalysis of quasielastic neutron scattering results. *AIP Conference Proceedings*, 1969(1):20002, 2018.

[60] Filippo Ferdeghini, Quentin Berrod, Jean-Marc Zanotti, Patrick Judeinstein, Victoria García Sakai, Orsolya Czakkel, Peter Fouquet, and Doru Constantin. Nanostructuration of ionic liquids: impact on the cation mobility. A multi-scale study. *Nanoscale*, 9(5):1901–1908, 2017.

[61] Andreas Schönhals Friedrich Kremer. *Broadband Dielectric Spectroscopy*. Springer-Verlag Berlin Heidelberg, 1 edition, 2003.

[62] Sverre Grimnes and Ørjan G Martinsen. Chapter 3 - dielectrics. In Sverre Grimnes and Ørjan G Martinsen, editors, *Bioimpedance and Bioelectricity*

Basics (Third Edition), pages 37 – 75. Academic Press, Oxford, third edition, 2015.

[63] Lauren Boldon, Fallon Laliberte, and Li Liu. Review of the fundamental theories behind small angle X-ray scattering, molecular dynamics simulations, and relevant integrated application. *Nano reviews*, 6:25661, feb 2015.

[64] Philip Willmott. *An Introduction to Synchrotron Radiation : Techniques and Applications*. John Wiley & Sons, Incorporated, 2019.

[65] Kinematical scattering I: non-crystalline materials, mar 2011.

[66] J. Als-Nielsen. *Diffraction, refraction and absorption of X-rays and neutrons: A comparative exposition*, chapter 1. Springer-Verlag Berlin Heidelberg, 1994.

[67] Quasielastic Neutron Scattering: An Advanced Technique for Studying the Relaxation Processes in Condensed Matter, 2016.

[68] G L Squires. *Introduction to the Theory of Thermal Neutron Scattering*. Cambridge University Press, Cambridge, 3 edition, 2012.

[69] Tatsiana Burankova, Juan F Mora Cardozo, Daniel Rauber, Andrew Wildes, and Jan P Embs. Linking Structure to Dynamics in Protic Ionic Liquids: A Neutron Scattering Study of Correlated and Single-Particle Motions. *Scientific Reports*, 8(1):16400, 2018.

[70] D. Richard, M. Ferrand, and G. J. Kearley. Analysis and visualisation of neutron-scattering data. *Journal of Neutron Research*, 4(1-4):33–39, 1996.

[71] Richard Tumanjong Azuah, Larry R Kneller, Yiming Qiu, Philip L W Tregenna-Piggott, Craig M Brown, John R D Copley, and Robert M Dimeo. DAVE: A Comprehensive Software Suite for the Reduction, Visualization, and Analysis of Low Energy Neutron Spectroscopic Data. *Journal of research of the National Institute of Standards and Technology*, 114(6):341–358, dec 2009.

[72] Marc Bée. *Quasielastic neutron scattering: principles and applications in solid state chemistry, biology and materials science*. IOP Publishing Ltd, Bristol, 1 edition, 1988.

[73] Quentin Berrod, Karine Lagrené, Jacques Ollivier, and Jean-Marc Zanotti. Inelastic and quasi-elastic neutron scattering. application to soft-matter. *EPJ Web of Conferences*, 188(05001), 2018.

[74] Hemant K Kashyap, Jeevapani J Hettige, Harsha V R Annapureddy, and Claudio J Margulis. SAXS anti-peaks reveal the length-scales of dual positive–negative and polar–apolar ordering in room-temperature ionic liquids. *Chem. Commun.*, 48(42):5103–5105, 2012.

[75] Alessandro Triolo, Olga Russina, Barbara Fazio, Giovanni Battista Appetecchi, Maria Carewska, and Stefano Passerini. Nanoscale organization in piperidinium-based room temperature ionic liquids. *The Journal of Chemical Physics*, 130(16):164521, apr 2009.

[76] K. Adrjanowicz, J. Pionteck, and M. Paluch. Isochronal superposition and density scaling of the intermolecular dynamics in glass-forming liquids with varying hydrogen bonding propensity. *RSC Adv.*, 6:49370–49375, 2016.

[77] F. Puosi, O. Chulkin, S. Bernini, S. Capaccioli, and D. Leporini. Thermodynamic scaling of vibrational dynamics and relaxation. *The Journal of Chemical Physics*, 145(23):234904, 2016.

[78] Michela Romanini, María Barrio, Roberto Macovez, María D Ruiz-Martin, Simone Capaccioli, and Josep Ll Tamarit. Thermodynamic Scaling of the Dynamics of a Strongly Hydrogen-Bonded Glass-Former. *Scientific reports*, 7(1):1346, may 2017.

[79] Henriette Wase Hansen, Bernhard Frick, Simone Capaccioli, Alejandro Sanz, and Kristine Niss. Isochronal superposition and density scaling of the α-relaxation from pico- to millisecond. *The Journal of Chemical Physics*, 149(21):214503, 2018.